ARTICLE

Circularly Polarized Laser with Chiral Nematic Cellulose Nanocrystal Cavity

Dan Qu, Matteo Archimi, Andrea Camposeo, Dario Pisignano,* and Eyal Zussman*

Read Online

ACCESS | Metrics & More | Article Recommendations | Supporting Information

ABSTRACT: Circularly polarized (CP) lasers derived from low-cost and renewable raw sources are attracting increasing attention in photonics and material science. Here, we present a facile and effective approach to fabricate CP lasers by the evaporation-induced assembly of cellulose nanocrystals (CNCs) and a laser dye. The obtained laser exhibits a controlled chiral nematic structure, which acts as a chiral optical cavity, and varied chiral coupling interactions. It is shown that the CNC-based laser can modify the polarization state of the laser into left-handed polarization, leading to strong CP laser emission (CPLE) with a dissymmetry factor up to 0.35. The chiral nematic CNC structure proves to be a versatile yet straightforward strategy to generate strong and tailored CPLE.

KEYWORDS: circularly polarized laser emission, chiral optical cavity, light-matter interaction, cellulose nanocrystal, chiral nematic structure
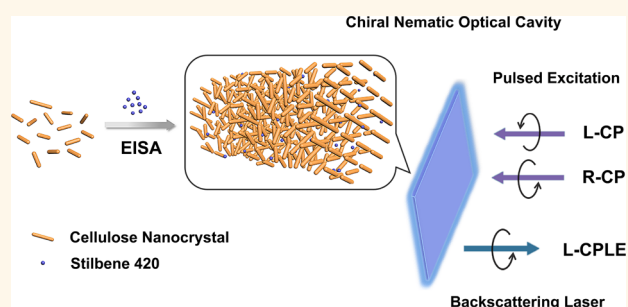
Circularly polarized (CP) lasers featuring significant prospects in advanced spectroscopic, communication, and display technologies are a burgeoning area in the field of photonics and material research.[1−4] Moreover, the CP laser is a powerful tool to investigate and understand the chirality-dependent light-matter interactions. The two basic requirements for CP laser emission (CPLE) are a laser gain medium and a chiral environment.[5−7] One strategy to enable CPLE is to use the intrinsic asymmetric structure of chiral organic molecules,[8] however, this strategy endows weak CPLE, and the high enantiopurity requirement raises the synthesis cost. Another method is based on the periodic spatial modulation of the refractive index of dye-doped media induced by interfering two CP beams from the same laser source.[9−11] This approach is challenging due to the complicated processing, while the resulted CPLE is relatively weak. Chiral nematic liquid crystals embedded with laser dyes that feature easy fabrication and wide-band tunability are becoming attractive since discovered by Kopp and co-workers.[1,2,12−15] However, a versatile strategy to develop cost-effective and strong CPLE at a large scale remains challenging.

A critical aspect in the design of CPLE, from an environmental and energy perspective, is selecting an eco-friendly, cheap, and well-conceived chiral optical cavity. When looking to nature for inspiration in chiral nematic solutions, representative examples are double helix structures in DNA segments, chitin-based helical microstructures in beetles, and helicoidal cellulose architectures in the fruit of *Pollia condensata*.[16−18] Cellulose is one of the most abundant and renewable biopolymers, transforming to cellulose nanocrystals (CNCs) upon controlled sulfuric acid hydrolysis.[19,20] CNCs have gained significant interest due to their capability to spontaneously self-assemble into a left-handed chiral nematic liquid crystalline phase in water. Such self-assembled CNCs retain a helix structure also at the solid-state (i.e., after water evaporation), which can be regarded as a one-dimensional photonic crystal.[21,22] When the light propagates along the direction parallel to the helix axis of CNCs, a selective reflection band occurs, which is also known as a photonic bandgap (PBG) for left-handed CP (L-CP) light. Attempts to explore the intriguing chiral nematic structures of CNCs have led to materials presenting passive and active CP light.[23−27] Walther and co-workers recently reported the laser emission arising from assembling CNCs and a dye in a polymer matrix,[28] however, the requirement to synthesize the dye-modified copolymer complicates the preparation process of the CNC-based laser array. Furthermore, the CNC-based materials act as a photonic structure cavity for the laser emission, and the
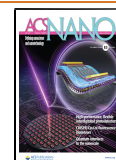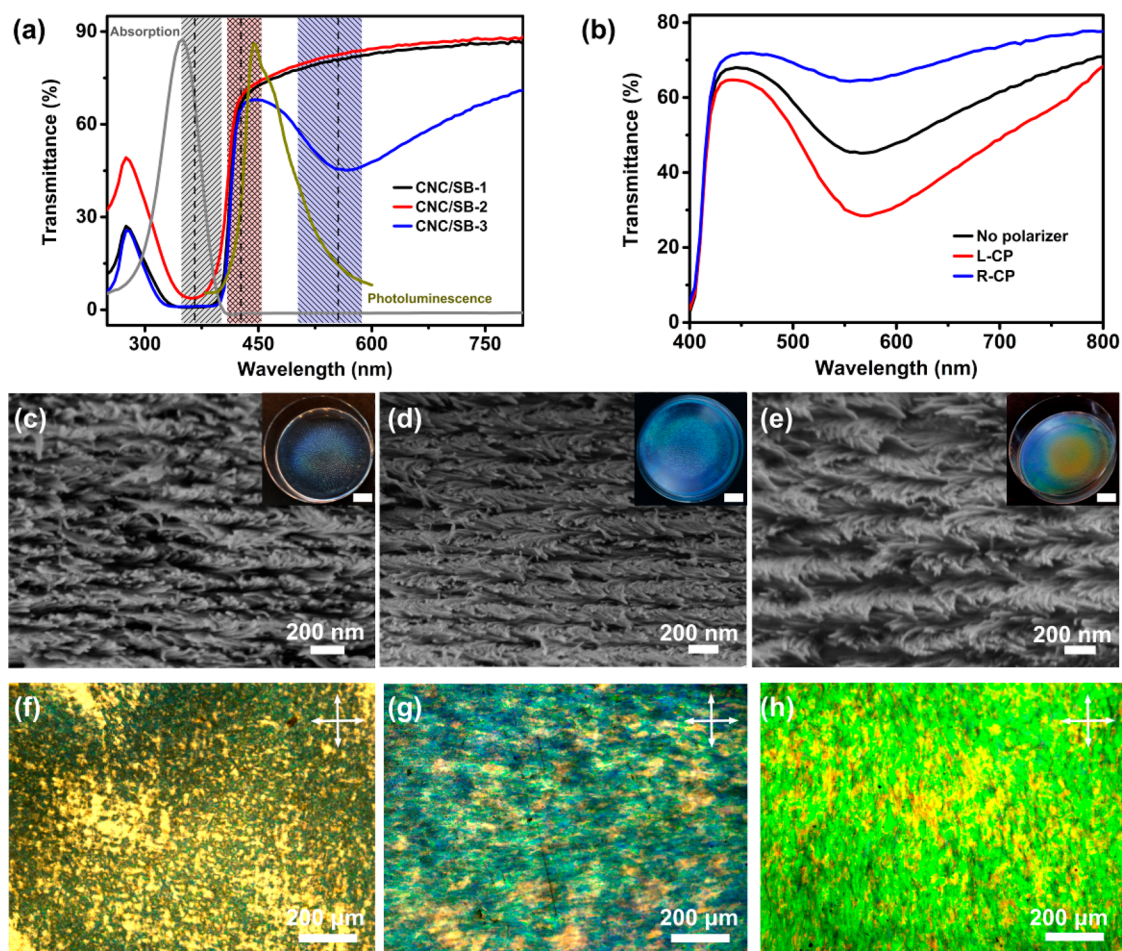
Figure 1. Chiral nematic composite films with different PBG assembled from CNCs and SB. (a) Transmission spectra of CNC/SB films showing the PBG overlap with the absorption of SB solution (gray line) for CNC/SB-1 and CNC/SB-2, and a clear PBG for the CNC/SB-3 film centered at 562 nm. The PBGs obtained from SEM data are displayed in the gray area for CNC/SB-1, red area for CNC/SB-2, and blue area for CNC/SB-3, respectively. The dashed line indicates the PBG average wavelength value. The fluorescent spectrum (dark yellow line) of SB aqueous solution (0.001 wt %) displaying an emission peak at 444 nm. (b) Transmission spectra of CNC/SB-3 film probed by L-CP, R-CP, and unpolarized light. (c–e) SEM images of CNC/SB-1, CNC/SB-2, and CNC/SB-3 samples, exhibiting periodical, layered order with different helix pitch and corresponding different reflective colors (insets, the scale bar is 1 cm). The images are taken in the vertical cross-section. (f–h) POM images of CNC/SB-1, CNC/SB-2, and CNC/SB-3 films obtained in reflection mode showing varied birefringence and planar textures (the crossed arrows indicate the axes of the analyzer and polarizer, respectively).

advantage of the chiral structure is not exploited. Thus, it will be attractive to use pristine CNCs as a chiral optical cavity to generate CPLE through a simple and efficient approach.

Herein, we design a strategy to fabricate CP lasers, based on the evaporation-induced self-assembly of CNCs, which act as a chiral optical cavity, and stilbene 420 (SB), selected as the gain compound. The water solubility of SB makes it possible to assemble with CNC aqueous suspension without destroying the chiral nematic structure. Meanwhile, the SB gain medium features high thermal and chemical stability and good laser efficiency. It is shown that the chiral nematic structure can strongly modify the emission of the dye, displaying angle-dependent CP emission. Tuning the helix pitch leads to manipulating the chiral PBG, which couples with the dye optical gain band, thus allowing different laser emission behaviors to be demonstrated. The composite chiral nematic film presents strong left-handed CPLE (L-CPLE) quantified by a dissymmetry factor of 0.35 when overlapping the PBG of the CNC structure sufficiently with dye emission and enhancing coupling effects. Our assembled chiral photonic CNC system offers an opportunity for the design and scalable preparation of

CPLE architectures from renewable sources without the need for expensive and tedious synthesis.

RESULTS AND DISCUSSION

Assembly of Chiral Optical Cavity. The CNCs used in this study are prepared from sulfuric acid hydrolysis of cotton pulp, exhibiting spindle-like shapes with a length of 196 ± 19 nm and a width of 14 ± 4 nm, as shown by transmission electron microscopy (Supporting Information (SI) Figure S1). The SB (molecular structure in SI Figure S2) displays an absorption band centered at a wavelength of 350 nm and emission in the 400−600 nm range, with a peak wavelength at 444 nm in water (Figure 1a). To maximize the coupling efficiency and enable laser emission with a low threshold in photonic crystals, the PBG should resonate well with the SB emission.[28−30] In our system, the optical properties of the composite films are tailored by controlling the CNC helix pitch while keeping constant the SB concentration (0.7 wt %). It is well-known that sonication is a straightforward tool to manipulate the helix pitch.[31] Thus, sonication for varying
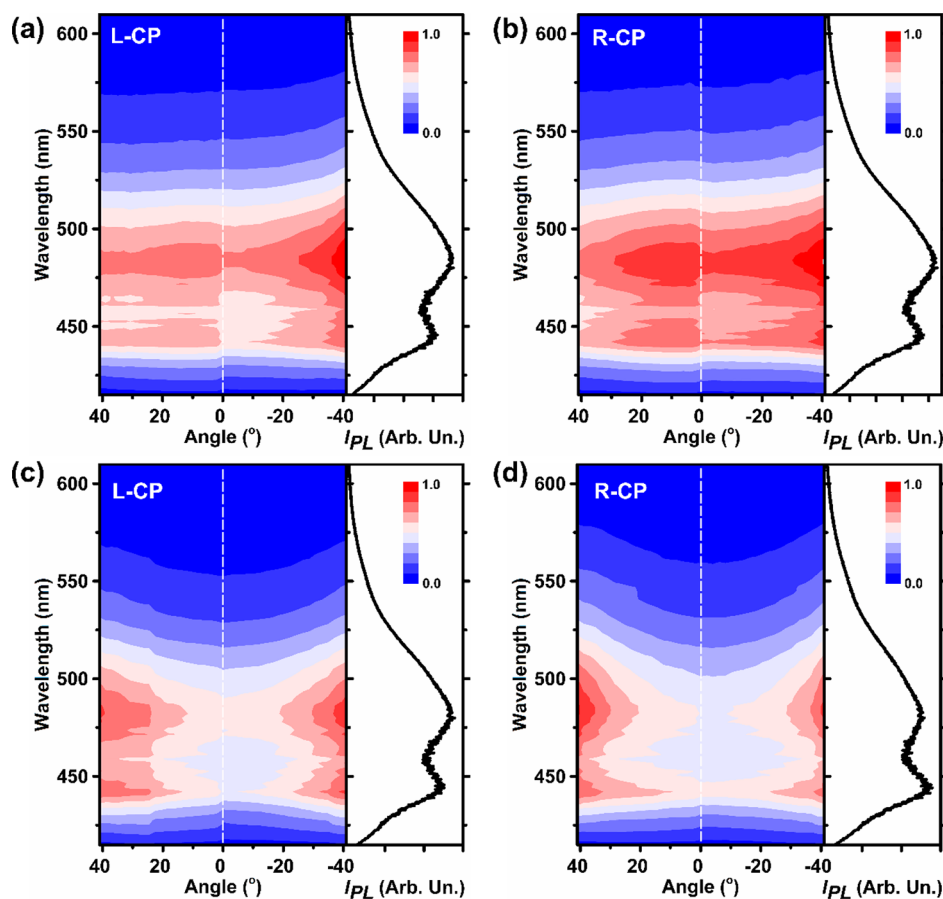
Figure 2. Angular-resolved, circularly polarized PL spectra of (a,b) CNC/SB-1 and (c,d) CNC/SB-2 film. The films are excited with an R-CP laser. Maps show the PL spectra with L-CP polarization [(a) and (c)], or with R-CP polarization [(b) and (d)]. The spectra collected at 0° (collection direction perpendicular to the sample surface, which is highlighted by the dashed lines in the maps) are shown on the right of each map.

time intervals is applied to the CNC suspension to control the helix pitch and the corresponding PBG in the obtained hybrid films (see Experimental Section).

Three exemplary composite and freestanding films, with thickness around 40 μm and different PBGs, are examined in the following. All the measurements are performed on the central regions of samples to minimize experimental errors associated with film-edge effects. The strong absorption of SB overlaps with the peak wavelength reflected by the chiral nematic CNC structure for the samples CNC/SB-1 and CNC/SB-2 (Figure 1a). Two prominent peaks are observed in the transmission spectrum of the CNC/SB-3 film. The first peak, within a range of 300−400 nm, is the absorption of SB; the second is centered at 562 nm, attributed to the selective reflection of the chiral nematic structure. The reflection spectra of the CNC/SB films are further analyzed to separate the reflection band of the chiral nematic structure from the SB absorption (SI Figure S3). The CNC/SB-2 and CNC/SB-3 films show reflection peaks at 430 and 558 nm, respectively, consisting of the transmittance results. CNC/SB-1 film shows a tiny peak at around 380 nm, likely due to overlapping with the increased reflectance at wavelength below 400 nm. As the PBG of the CNC/SB-3 film is far from the SB absorption, it is used as an example to detect the polarization state of the reflected light. The transmittance from the chiral nematic CNC structure decreases when using a L-CP incident light and increases when using a right-handed CP (R-CP) incident light,

indicating the selective reflection of L-CP light and transmission of R-CP light (Figure 1b). Scanning electron microscopy (SEM) inspection is performed to correlate the central wavelength (λ) of the PBG with the helix pitch, according to the relation: $\lambda = nP$, where n is the average refractive index of the composite film ($n = 1.54$) and P is the helix pitch.[22,32] Cross-section SEM images of CNC/SB films display long-range ordered, periodical, and left-handed chiral nematic structure with a helix CNC arrangement (Figure 1c–e, SI Figure S4). The CNC/SB-1 film shows a pitch of 235 ± 12 nm. Upon increasing the sonication time, the pitch increases. The CNC/SB-2 film exhibits a pitch of 276 ± 11 nm, and the CNC/SB −3 film displays a pitch of 361 ± 14 nm. Correspondingly, the PBG determined from the measured pitch is centered at 363 ± 12 nm and 425 ± 11 nm for CNC/SB-1 and CNC/SB-2, respectively, matching well with the reflection spectra and the SB absorption (PBGs obtained from the SEM images are also highlighted in Figure 1a). For the CNC/SB-3 film, the PBG calculated from the SEM analysis (556 ± 14 nm) is in good agreement with the measured peaks in the optical transmission and reflection spectra. The macroscopic reflectance color of the film changes from light blue to green, determined by the pitch increase from CNC/SB-1 to CNC/SB-3. Besides, polarized optical microscopy (POM) images evidence strong birefringence and planar textures for all the films, confirming the helix axis being perpendicular to the film surface (Figure 1f–h). The fingerprint textures are also
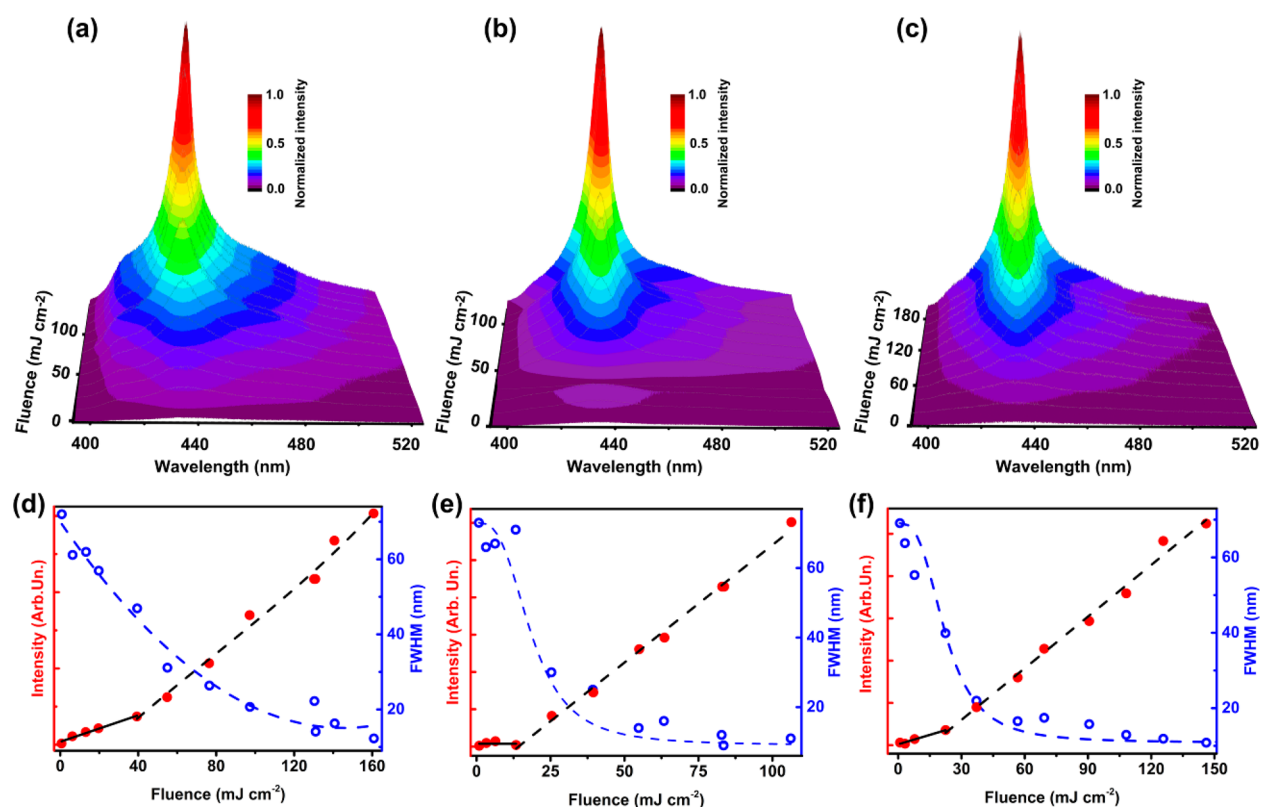
Figure 3. 3D emission intensity maps showing the spectra of (a) CNC/SB-1, (b) CNC/SB-2, and (c) CNC/SB-3 as a function of incident excitation fluence, respectively. (d) Light-out vs light-in curve (full red dots, left axis) of CNC/SB-1, showing a smooth transition upon increasing the excitation fluence, indicating amplified spontaneous emission. The decrease of the emission spectral line-width, which is calculated as the full width at half-maximum (FWHM) of the spectra, upon increasing the excitation fluence (empty blue dots, right axis), is also shown. (e,f) Light-out vs light-in plot (full red dots, left axis) of CNC/SB-2 and CNC/SB-3 film and a decrease of FWHM upon increasing the excitation fluence (empty blue dots, right axis), indicating the laser emission. The black dashed and continuous lines are fit to the data above and below the lasing threshold, respectively. The blue dashed lines are guides for the eyes.

observed during the drying process of CNC/SB suspensions, confirming chiral nematic structure formation (SI Figure S5). Some fingerprint textures are also observed in the high-resolution POM images of CNC/SB films, indicating certain defects are formed in the chiral photonic films (SI Figure S6). Overall, these findings are associated with the formation of the chiral nematic structure in solid-state composite films, which is essential for realizing a chiral optical cavity for lasers.

Angular-Resolved CP Emission of the Chiral Photonic Films. The angular-dependent spontaneous emission of CNC/SB, decomposed into L- and R-CP contributions, is first investigated. For the CNC/SB-1 film, when collected perpendicular to the film surface, the shape of the R-CP and L-CP photoluminescence (PL) spectrum is almost unchanged, which is found upon excitation with both R-CP and L-CP laser light (Figure 2a,b, SI Figure S7a,b). This is due to the PBG, which is nearly outside the SB luminescence, leading to poorly efficient optical coupling. Upon increasing the collecting angle, the PBG blue shifts far away from the SB emission, giving rise to almost unperturbed PL. For CNC/SB-2, an apparent variation of the PL spectrum is instead observed in the L-CP and R-CP emission (Figure 2c,d, SI Figure S7c,d).[33] This is an indication of an interplay between the light emitted by the incorporated SB and the chiral photonic structure formed by the CNC. For instance, one clearly sees for PL collected at 0° (i.e., perpendicular to the sample surface), that the shape of the L-CP emission spectrum is different from that of the R-CP one: in particular, for the L-CP emission, the peak at 444 nm is

weaker than that at 480 nm, whereas the peak at 444 nm is higher than that at 480 nm for the R-CP emission (Figure 2c,d). Here, the PBG of the CNC structure overlaps largely with the spontaneous emission of SB. As a consequence, the L-CP emission at 444 nm is suppressed with respect to the emission at a longer wavelength (480 nm). In contrast, for the R-CP emission spectrum, on which the left-handed chiral nematic structure has a minor impact, the emission at 444 nm is enhanced compared to that at 480 nm, likely arising from the slow-photon effect[34] where the photon velocity reduces and photon dwell time increases at the photonic band edge (Figure 2d). The PBG of the CNC/SB-2, which blue shifts when increasing the angle (Figure S8), covers the excitation wavelength of 410 nm at the angle of 0°−24°. At a measurement angle of around 0°−24°, the L-CP incident light at 410 nm is reflected by CNC/SB-2 film, and fewer can enter the sample to excite the SB molecule; while R-CP incident light is not affected. Meanwhile, the R-CP emission is barely reflected by the chiral nematic structure. As a result, the R-CP emission intensity of CNC/SB-2 when excited by L-CP light is lower than that of R-CP light. At a measurement angle of around 24°−40°, the emission intensity of CNC/SB-2 excited by L- or R-CP light is more or less the same (Figure 2d, SI Figure S7d). These different behaviors would determine different lasing properties.

Lasing Properties of the Chiral Photonic Films. The lasing properties of CNC/SB films are investigated using the third harmonic of an Nd:YAG pulsed laser (emission

wavelength 355 nm, pulse duration 10 ns, and linear polarization), while the emission is collected in a back-scattering configuration. When pumped by intense excitation, the population inversion takes place in the SB gain medium, leading to stimulated emission from the dye embedded in the CNC optical cavity, and ultimately to lasing. The defects in the assembled chiral nematic composite CNC film might act as scattering sites for emission out-coupling. The emission intensity of CNC/SB-1, where the emission spectrum is located nearly outside the PBG, increases upon with increasing the excitation fluence (Figure 3a,d, Table 1). The light-out vs

Table 1. Summary of the Properties Measured upon Pulsed Laser Excitation for the Various CNC/SB Films

sample no.	PBG central wavelength determined from SEM data (nm)	excitation threshold for line-narrowing (mJ cm^{-2})	wavelength of the emission peak (nm)	minimum value of the FWHM (nm)
CNC/SB-1	363	40	435.4	12
CNC/SB-2	425	13	434.6	9
CNC/SB-3	556	28	434.4	10

light-in curve exhibits a smooth transition from the spontaneous emission to a brighter one with an estimated threshold at about 40 mJ cm^{-2}, while the emission intensity has a nonlinear threshold and is weakly dependent on the excitation fluence, which is indicative of amplified spontaneous emission.[35] Moreover, the emission of CNC/SB-1 film features a smooth decrease of the spectral line-width, which is calculated as the full width at half-maximum (FWHM) of the spectra when increasing the excitation fluence. In contrast, the CNC/SB-2 sample (where the emission spectrum overlaps well with the PBG) displays a broad luminescence spectrum

when excited at 3.3 mJ cm^{-2} and a clear peak emerges when increasing the excitation fluence above the threshold value of 13 mJ cm^{-2} (Figure 3b,e, Table 1). A clear transition at the threshold of 13 mJ cm^{-2} is found, above which a linear increase of the output intensity is measured in the light-out vs light-in data, as well as a sharp decrease of the spectral line-width (Figure 3e), strongly supporting the occurrence of laser emission. The CNC/SB-2 film displays a minimum FWHM of 9 nm, indicative of multimode lasing, likely due to the overlap of various emission peaks arising from local PBG dissimilarity of the CNC structure within the area of the excitation spot, as also observed in another report.[28] Indeed, spatially resolved spectra of the film measured by laser confocal fluorescence microscopy show a variation of the emission spectra over areas of the order of tens of micrometers (SI Figure S9), which is attributable to the local pitch distribution of the chiral nematic CNC domain. Such CNC assembly may also result in laser emission from defect modes[36] and random lasing,[37] which can both contribute to the observed broadband laser emission. An efficient interplay displays between the light emitted by the incorporated SB and chiral nematic structure in the CNC/SB-2 film as confirmed in the angular-resolved luminescent spectra, thus leading to lasing emission with a low threshold. Such interplay is not observed in CNC/SB-1 film, which is in line with the amplified spontaneous emission with a much higher estimated threshold instead of lasing emission.

The laser emission of CNC/SB-3 film where the emission spectrum locates further away from PBG is also investigated to study the effect of the PBG position on the lasing properties. A sharp lasing emission with a minimum FWHM of 10 nm is observed upon increasing the pump fluence above the threshold of 28 mJ cm^{-2} for CNC/SB-3 film (Figure 3c,f). The less efficient laser emission is attributed to the reduced resonator quality, arising from the less sufficient overlap between the PBG of the CNC and the luminescence spectrum
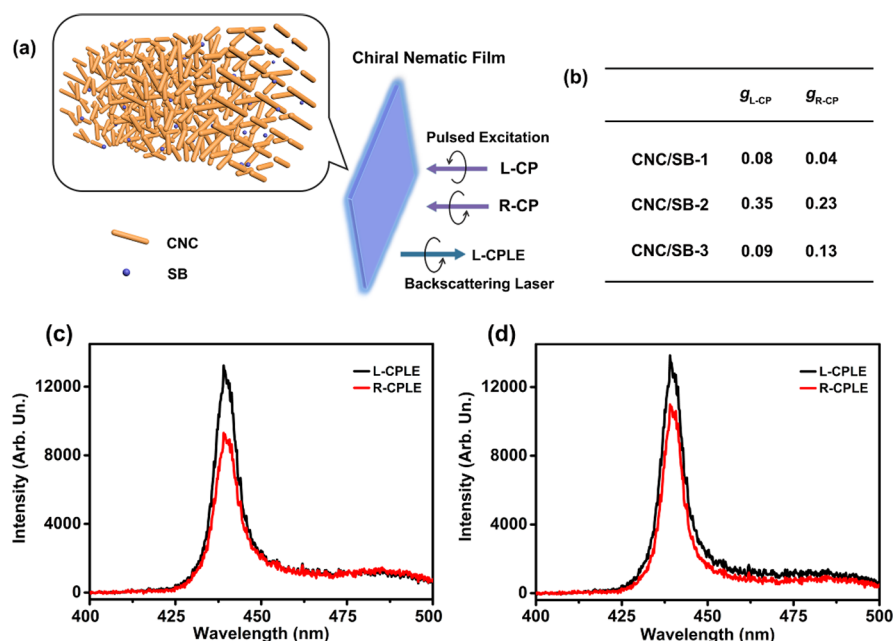

Figure 4. (a) Illustration of CNC-based CPLE: overlap of the PBG of the left-handed chiral nematic CNC/SB film with the luminescence of SB, enabling L-CPLE when excited by L-CP or R-CP laser light. (b) Summary of dissymmetry factor g_{L-CP} when the system is excited by L-CP laser and g_{R-CP} when excited by R-CP laser. L-CPLE and R-CPLE spectra of CNC/SB-2 film upon excitation (excitation fluence = 90 mJ cm^{-2}) with (c) L-CP and (d) R-CP laser, showing the main component of L-CPLE.

of SB (Table 1). The lasing emission peak of CNC/SB films staying almost the same is likely a result of the relatively broad PBG that overlaps with the emission of SB.

To investigate the pristine CNC contribution to the observed lasing behavior, the lasing properties of the CNC film are characterized using the same experimental setup for CNC/SB laser tests (SI Figure S10). The emission spectra of pristine CNC and CNC/SB-2 are compared at various excitation fluences. The signal measured for the pristine CNC at the CNC/SB-2 emission peak is 3 orders of magnitude lower at the lower excitation fluence and about a factor 3×10^{-4} lower at the excitation fluence of 80 mJ cm^{-2}. Such results evidence a dominant contribution of the SB emission to the lasing in the range of investigated wavelengths.

CPLE Properties of Chiral Photonic Films. Given the chiral photonic structure, the resulting laser emission polarization state of the composite CNC/SB film is then studied (Figure 4). An either L-CP or R-CP excitation beam is realized by a linearly polarized input laser combined with a $\lambda/4$ waveplate, while the polarization state of the emission is analyzed by means of L-CP and R-CP filters, positioned in front of the collection optical fiber. Taking CNC/SB-2 films as an example, the L-CPLE and right-handed CPLE (R-CPLE) spectra are collected by pumping either by the L-CP or by the R-CP excitation laser beam. The CNC/SB-2 film shows a main component of L-CPLE, regardless of the specific excitation (L-CP or R-CP laser, Figure 4a). To quantify the polarization degree of the laser output, the dissymmetry factor, g, is used:[38,39]

$$g = \frac{I_L - I_R}{\frac{1}{2}(I_L + I_R)} \tag{1}$$

where I_L, I_R denote the intensities of the emitted L-CP and R-CP light, respectively. For a perfect chiral photonic structure, the maximum $|g|$ is 2. A positive (negative) dissymmetry factor indicates that the output radiation is left-handed (right-handed). The output laser is left-handed primarily, consistent with the handedness of the chiral photonic CNC cavity. The corresponding g value is 0.35 and 0.23 for L-CP and R-CP excitation, respectively (Figure 4b−d). Since SB molecules are randomly distributed in the composite film, the CNC/SB film behaves like an isotropic medium in the photoexcitation process of SB, and its behavior is therefore independent of the polarization of the pumping laser. Owing to the left-handed chiral nematic structure, the CNC/SB film can selectively reflect L-CP light and transmit R-CP light in the reflection photonic band. Hence, the pumped L-CP laser may be affected in the reflection band, and the pumped R-CP laser can transmit without loss. Indeed, the PBG (425 nm) of the CNC/SB-2 film at normal incidence does not cover the pumping wavelength, leading to no loss of the L-CP excitation light induced by the reflection of the CNC photonic structure. The laser emission centered at 435.4 nm is inside the reflection band of the left-handed chiral photonic composite film; thus, the L-CPLE is reflected, while the R-CPLE is barely affected and mainly transmitted through the CNC photonic structure, leading to a positive g when detected in a backscattering configuration. These results are also supported by the behavior of CNC/SB-3 films, which display less efficient L-CPLE and a g of 0.09 and 0.13 when excited by L-CP and R-CP laser, respectively. This is in line with the less efficient coupling between the chiral photonic structure and the SB emission

(Figure 4b, SI Figure S11c,d). Finally, when excited by either L-CP or R-CP input laser, CNC/SB-1 films show almost unpolarized emission with the corresponding dissymmetry factor of 0.08 and 0.04, as the PBG of the CNC structure is nearly outside the luminescence of SB (Figure 4b, SI Figure S11a,b). The PBG of CNC/SB-1 film covers the pump light at 355 nm. Thus, the L-CP excitation laser is partly reflected, and fewer photons in the left polarization can enter the sample to excite the SB molecule; while the R-CP excitation laser is not affected. Hence, the emission intensity excited by L-CP laser light is weaker than that excited by R-CP light (SI Figure S11a,b). CNC/SB-2 film exhibits the strongest L-CPLE, which matches the most apparent different L- and R-CP emission in the angular-resolved luminescence. Overall, these findings highlight how sensitive these architectures are in terms of resulting CPLE, which depends on the CNC pitch and assembly in such a way that tight control and tailored CP behavior can be obtained.

CONCLUSIONS

In conclusion, we have uncovered the potential of chiral nematic CNC structures acting as a chiral optical cavity to fabricate CP lasers. It is shown that the chiral photonic structure can modify the emission due to its coupling interaction with dye emission. The laser can be tuned by manipulating the helix pitch of the CNC, reaching a threshold of 13 mJ cm^{-2}. A CNC-based CP laser architecture that displays L-CPLE arising from the selective reflection of L-CP light is realized. By varying the assembled laser dye, it is expected that one can build CP laser arrays covering a wide wavelength range of CPLE. The evaporation-induced assembly is a versatile and straightforward strategy, with potential for both rational design and scaled-up production of CPLE materials. The current results in this work are proof-of-concept. Further studies are needed to inspect the critical issues such as the parameters leading to strong CPLE, the evaporation speed, CNC concentration, and the thickness of the film. It is envisaged that chiral photonic cellulose materials will render them promising candidates in next-generation photonics relying on renewable, bioinspired materials.

EXPERIMENTAL SECTION

Materials. Cotton pulp board was obtained from Hebei Paper Group of China. Sulfuric acid (H$_2$SO$_4$, 98 wt %) was purchased from Bio-Lab Ltd.. SB was purchased from Exciton Inc.. Sodium hydroxide was ordered from Frutarom Ltd.. All chemicals were used as received without further purification. The deionized water was used for all experiments.

Preparation of the Chiral Nematic CNC/SB Films. The CNC aqueous suspension was prepared according to our previous report.[24] A 4 wt % CNC suspension was adjusted to pH 7 using a 5 wt % NaOH solution. Two 20 mL CNC suspensions were added to two 50 mL vials and sonicated for 9 and 20 s in an ice bath using 20% amplitude to get two CNC suspensions with different pitches. 850 μL 0.1 wt % SB aqueous solution was added separately to a 3 mL CNC suspension with sonication time of 0, 9, and 20 s and stirred at room temperature for 90 min. The suspensions were poured into 5 mL polystyrene Petri dishes and allowed to dry for 2 days at ambient environment. The SB concentration in the final obtained film was 0.7 wt %, and the thickness of the hybrid film was around 40 μm.

Material Characterization. The size of the CNC nanorod was analyzed by transmission electron microscopy using an FEI Tecnai G2S-Twin F20 system with a field emission gun operating at 200 kV. The absorption spectra of the SB solution and transmittance of composite CNC/SB films were measured by a Thermo Scientific

Genesys 10 UV Spectrophotometer. The films were mounted perpendicular to the beam path. The transmittance of the left- and right-handed circularly polarized light for the composite film was probed using left- and right-handed circularly polarized filters in the range of 400−700 nm. The reflectance of the CNC/SB films were detected on Cary 5000 UV−vis-NIR spectrophotometer, equipped with an integrating sphere, in reflection mode. The cross-section scanning electron microscopy (SEM) analysis of the composite CNC/SB films was performed by a Zeiss Ultra Plus microscope at an accelerating voltage of 3 kV. The films were coated with a thin layer of carbon. Polarized optical microscopy (POM) images were obtained using Olympus BX51-P microscope with crossed polarizers.

Confocal Microscopy. Fluorescence confocal microscopy was carried out using an inverted microscope equipped with a confocal laser scanning head (FV1000, Olympus). Samples were excited by a diode laser (emission wavelength 405 nm), which was focused onto the sample surface by a 20× objective with numerical aperture, NA = 0.75. The sample luminescence was collected by the same objective, and the emission intensity was measured by a photomultiplier. The spatially resolved luminescent spectra were measured by collecting fluorescence micrographs at various emission wavelengths with a spectral bandwidth of 2 nm.

Angle-Resolved Photoluminescence. The angle-resolved photoluminescence maps were obtained by collecting the emission spectra of the sample along various directions with respect to the axis perpendicular to the sample surface, which corresponds to 0°. To this aim, the samples were excited by a continuous wave, linearly polarized diode laser with an emission wavelength of 410 nm and spot size of about 1 mm. The polarization of the excitation laser was changed between left, and right circular polarization by means of a $\lambda/4$ waveplate mounted on a rotation stage. The emission of the samples was collected by a multimode optical fiber coupled to a monochromator (USB4000, Ocean Optics). To obtain angle-resolved emission spectra, the optical fiber was mounted on a rotation stage, and emission spectra were collected with steps of 2°. The polarization state of the emission was measured by left and right circular polarization filters (Thorlabs), positioned between the sample and the collection optical fiber.

Laser Measurements. For the characterization of the lasing properties of the assembled chiral photonic CNC/SB, the samples which are mounted in a vacuum chamber, with a background pressure of 10^{-5} mbar were excited by the third harmonic of an Nd:YAG pulsed laser (emission wavelength 355 nm, pulse duration 10 ns, and linear polarization). The excitation beam was directed onto the sample surface through a dichroic mirror, with an incident direction perpendicular to the sample surface (spot size 300 μm), while the emission was collected in backscattering configuration by a lens and coupled to a multimode optical fiber. The emission spectra were analyzed by a monochromator (iHR320, Jobin Yvon) equipped with a charged coupled device detector. The polarization of the excitation beam was varied from linear to left and right circular polarization by means of a $\lambda/4$ waveplate, while the polarization of the emission was analyzed by means of left and right circular polarization filters (Thorlabs), positioned in front of the collection optical fiber.

ASSOCIATED CONTENT

Ⓢ Supporting Information

The Supporting Information is available free of charge at https://pubs.acs.org/doi/10.1021/acsnano.1c01001.

> TEM image of CNCs; the molecular structure of SB; SEM images and reflectance spectra of CNC/SB films; POM images of CNC/SB suspensions and films; angle-resolved CP emission spectra of CNC/SB films when excited by L-CP light; angle-dependent PBG of CNC/SB films; fluorescence confocal micrograph of a CNC/SB-2 film; the lasing properties of pristine CNC; L-CP and R-CP emission spectra of CNC/SB-1 upon excitation with L-CP and R-CP laser; L-CPLE and R-CPLE spectra of CNC/SB-3 upon excitation with L-CP and R-CP laser (PDF)

AUTHOR INFORMATION

Corresponding Authors

Dario Pisignano − *Dipartimento di Fisica, Università di Pisa, I-56127 Pisa, Italy; NEST, Istituto Nanoscienze-CNR and Scuola Normale Superiore, I-56127 Pisa, Italy;* ⓞ orcid.org/0000-0003-3758-5199; Email: dario.pisignano@unipi.it

Eyal Zussman − *NanoEngineering Group, Faculty of Mechanical Engineering, Technion-Israel Institute of Technology, Haifa 3200003, Israel;* ⓞ orcid.org/0000-0002-4310-6548; Email: meeyal@technion.ac.il

Authors

Dan Qu − *NanoEngineering Group, Faculty of Mechanical Engineering, Technion-Israel Institute of Technology, Haifa 3200003, Israel;* ⓞ orcid.org/0000-0001-7075-2505

Matteo Archimi − *Dipartimento di Fisica, Università di Pisa, I-56127 Pisa, Italy*

Andrea Camposeo − *NEST, Istituto Nanoscienze-CNR and Scuola Normale Superiore, I-56127 Pisa, Italy;* ⓞ orcid.org/0000-0002-3533-7389

Complete contact information is available at:
https://pubs.acs.org/10.1021/acsnano.1c01001

Notes

The authors declare no competing financial interest.

REFERENCES

(1) Coles, H.; Morris, S. Liquid-Crystal Lasers. *Nat. Photonics* **2010**, *4*, 676−685.

(2) Furumi, S. Recent Progress in Chiral Photonic Band-Gap Liquid Crystals for Laser Applications. *Chem. Rec.* **2010**, *10*, 394−408.

(3) Lindemann, M.; Xu, G.; Pusch, T.; Michalzik, R.; Hofmann, M. R.; Žutić, I.; Gerhardt, N. C. Ultrafast Spin-Lasers. *Nature* **2019**, *568*, 212−215.

(4) Adamow, A.; Szukalski, A.; Sznitko, L.; Persano, L.; Pisignano, D.; Camposeo, A.; Mysliwiec, J. Electrically Controlled White Laser Emission through Liquid Crystal/Polymer Multiphases. *Light: Sci. Appl.* **2020**, *9*, 1−9.

(5) Cerdán, L.; García Moreno, S.; Costela, A.; García Moreno, I.; de la Moya, S. Circularly Polarized Laser Emission Induced in Isotropic and Achiral Dye Systems. *Sci. Rep.* **2016**, *6*, 28740.

(6) Cerdán, L.; Moreno, F.; Johnson, M.; Muller, G.; de la Moya, S.; García Moreno, I. Circularly Polarized Laser Emission in Optically Active Organic Dye Solutions. *Phys. Chem. Chem. Phys.* **2017**, *19*, 22088−22093.

(7) Yokoyama, S.; Mashiko, S.; Kikuchi, H.; Uchida, K.; Nagamura, T. Laser Emission from a Polymer-Stabilized Liquid-Crystalline Blue Phase. *Adv. Mater.* **2006**, *18*, 48−51.

(8) Jiménez, J.; Cerdán, L.; Moreno, F.; Maroto, B. L.; García Moreno, I.; Lunkley, J. L.; Muller, G.; de la Moya, S. Chiral Organic Dyes Endowed with Circularly Polarized Laser Emission. *J. Phys. Chem. C* 2017, *121*, 5287−5292.

(9) Chen, F.; Gindre, D.; Nunzi, J. M. Tunable Circularly Polarized Lasing Emission in Reflection Distributed Feedback Dye Lasers. *Opt. Express* 2008, *16*, 16746−16753.

(10) Lo, D.; Ye, C.; Wang, J. Distributed Feedback Laser Action by Polarization Modulation. *Appl. Phys. B: Lasers Opt.* 2003, *76*, 649−653.

(11) Ye, C.; Wang, J.; Shi, L.; Lo, D. Polarization and Threshold Energy Variation of Distributed Feedback Lasing of Oxazine Dye in Zirconia Waveguides and in Solutions. *Appl. Phys. B: Lasers Opt.* 2004, *78*, 189−194.

(12) Kopp, V. I.; Fan, B.; Vithana, H. K. M.; Genack, A. Z. Low-Threshold Lasing at the Edge of a Photonic Stop Band in Cholesteric Liquid Crystals. *Opt. Lett.* 1998, *23*, 1707−1709.

(13) Gardiner, D. J.; Morris, S. M.; Hands, P. J. W.; Mowatt, C.; Rutledge, R.; Wilkinson, T. D.; Coles, H. J. Paintable Band-Edge Liquid Crystal Lasers. *Opt. Express* 2011, *19*, 2432−2439.

(14) Choi, H. J.; Bae, J. H.; Bae, S.; Lee, J. J.; Nishikawa, H.; Araoka, F.; Choi, S. W. Development of a Liquid Crystal Laser Using a Simple Cubic Liquid Crystalline Blue Phase Platform. *RSC Adv.* 2019, *9*, 32922−32927.

(15) Lee, S.; Jeong, Y. In Random Laser from Beetle Elytral Surface with Circularly Polarized Light Emission, *Frontiers in Optics + Laser Science APS/DLS*, Washington, DC, 2019/09/15; Optical Society of America: Washington, DC, 2019; p JTu3A.51.

(16) De Michele, C.; Zanchetta, G.; Bellini, T.; Frezza, E.; Ferrarini, A. Hierarchical Propagation of Chirality through Reversible Polymerization: The Cholesteric Phase of DNA Oligomers. *ACS Macro Lett.* 2016, *5*, 208−212.

(17) Sharma, V.; Crne, M.; Park, J. O.; Srinivasarao, M. Structural Origin of Circularly Polarized Iridescence in Jeweled Beetles. *Science* 2009, *325*, 449−451.

(18) Vignolini, S.; Rudall, P. J.; Rowland, A. V.; Reed, A.; Moyroud, E.; Faden, R. B.; Baumberg, J. J.; Glover, B. J.; Steiner, U. Pointillist Structural Color in Pollia Fruit. *Proc. Natl. Acad. Sci. U. S. A.* 2012, *109*, 15712−15715.

(19) Habibi, Y.; Lucia, L. A.; Rojas, O. J. Cellulose Nanocrystals: Chemistry, Self-Assembly, and Applications. *Chem. Rev.* 2010, *110*, 3479−3500.

(20) Moon, R. J.; Martini, A.; Nairn, J.; Simonsen, J.; Youngblood, J. Cellulose Nanomaterials Review: Structure, Properties and Nanocomposites. *Chem. Soc. Rev.* 2011, *40*, 3941−3994.

(21) Revol, J. F.; Bradford, H.; Giasson, J.; Marchessault, R. H.; Gray, D. G. Helicoidal Self-Ordering of Cellulose Microfibrils in Aqueous Suspension. *Int. J. Biol. Macromol.* 1992, *14*, 170−172.

(22) Shopsowitz, K. E.; Qi, H.; Hamad, W. Y.; MacLachlan, M. J. Free-Standing Mesoporous Silica Films with Tunable Chiral Nematic Structures. *Nature* 2010, *468*, 422−425.

(23) Zheng, H.; Li, W.; Li, W.; Wang, X.; Tang, Z.; Zhang, S. X. A.; Xu, Y. Uncovering the Circular Polarization Potential of Chiral Photonic Cellulose Films for Photonic Applications. *Adv. Mater.* 2018, *30*, 1705948.

(24) Qu, D.; Zheng, H.; Jiang, H.; Xu, Y.; Tang, Z. Chiral Photonic Cellulose Films Enabling Mechano/Chemo Responsive Selective Reflection of Circularly Polarized Light. *Adv. Opt. Mater.* 2019, *7*, 1801395.

(25) Xu, M.; Wu, X.; Yang, Y.; Ma, C.; Li, W.; Yu, H.; Chen, Z.; Li, J.; Zhang, K.; Liu, S. Designing Hybrid Chiral Photonic Films with Circularly Polarized Room-Temperature Phosphorescence. *ACS Nano* 2020, *14*, 11130−11139.

(26) He, J.; Bian, K.; Li, N.; Piao, G. Generation of Full-Color and Switchable Circularly Polarized Luminescence from Nonchiral Dyes Assembled in Cholesteric Cellulose Films. *J. Mater. Chem. C* 2019, *7*, 9278−9283.

(27) Tao, J.; Zou, C.; Jiang, H.; Li, M.; Lu, D.; Mann, S.; Xu, Y. Optically Ambidextrous Reflection and Luminescence in Self-Organized Left-Handed Chiral Nematic Cellulose Nanocrystal Films. *CCS Chem.* 2021, *3*, 932−945.

(28) Guo, J.; Haehnle, B.; Hoenders, D.; Creusen, G.; Jiao, D.; Kuehne, A. J.; Walther, A. Biodegradable Laser Arrays Self-Assembled from Plant Resources. *Adv. Mater.* 2020, *32*, 2002332.

(29) Ilchyshyn, I.; Tikhonov, E. How Laser Physics Brought Optics to the World of Photonic Crystals. *Ukr. J. Phys.* 2020, *65*, 327−327.

(30) Ford, A. D.; Morris, S. M.; Coles, H. J. Photonics and Lasing in Liquid Crystals. *Mater. Today* 2006, *9*, 36−42.

(31) Beck, S.; Bouchard, J.; Berry, R. Controlling the Reflection Wavelength of Iridescent Solid Films of Nanocrystalline Cellulose. *Biomacromolecules* 2011, *12*, 167−172.

(32) de, H. Rotatory Power and Other Optical Properties of Certain Liquid Crystals. *Acta Crystallogr.* 1951, *4*, 219−226.

(33) Risse, A. M.; Schmidtke, J. Angular-Dependent Spontaneous Emission in Cholesteric Liquid-Crystal Films. *J. Phys. Chem. C* 2019, *123*, 2428−2440.

(34) Figotin, A.; Vitebskiy, I. Slow Light in Photonic Crystals. *Waves Random Complex Media* 2006, *16*, 293−382.

(35) Svelto, O.; Taccheo, S.; Svelto, C. Analysis of Amplified Spontaneous Emission: Some Corrections to the Linford Formula. *Opt. Commun.* 1998, *149*, 277−282.

(36) Schmidtke, J.; Stille, W.; Finkelmann, H. Defect Mode Emission of a Dye Doped Cholesteric Polymer Network. *Phys. Rev. Lett.* 2003, *90*, No. 083902.

(37) Germano, G. C. M.; Machado, Y. D. R.; Martinho, L.; Fernandes, S. N.; Costa, A. M. L. M.; Pecoraro, E.; Gomes, A. S. L.; Carvalho, I. C. S. Flexible Random Lasers in Dye-Doped Bio-Degradable Cellulose Nanocrystalline Needles. *J. Opt. Soc. Am. B* 2020, *37*, 24−29.

(38) Riehl, J. P.; Richardson, F. S. Circularly Polarized Luminescence Spectroscopy. *Chem. Rev.* 1986, *86*, 1−16.

(39) Yu, C. L.; Hsiao, Y. H.; Chang, C. Y.; Cheng, P. J.; Lin, H. T.; Lai, M. S.; Kuo, H. C.; Chang, S. W.; Shih, M. H. High Circular Polarized Nanolaser with Chiral Gammadion Metal Cavity. *Sci. Rep.* 2020, *10*, 7880.